

A new spin on disks of satellite galaxies

Marius Cautun^{1*}, Wenting Wang¹, Carlos S. Frenk¹ and Till Sawala¹

¹ *Department of Physics, Institute for Computational Cosmology, University of Durham, South Road Durham DH1 3LE, UK*

7 December 2024

ABSTRACT

We investigate the angular and kinematic distributions of satellite galaxies around a large sample of bright isolated primaries in the spectroscopic and photometric catalogues of the Sloan Digital Sky Survey (SDSS). We detect significant anisotropy in the spatial distribution of satellites. To test whether this anisotropy could be related to the rotating disks of satellites recently found by Ibata et al. in a sample of SDSS galaxies, we repeat and extend their analysis. Ibata et al. found an excess of satellites on opposite sides of their primaries having anticorrelated radial velocities. We find that this excess is sensitive to small changes in the sample selection criteria which can greatly reduce its significance. In addition, we find no evidence for correspondingly correlated velocities for satellites observed on the same side of their primaries, which would be expected for rotating disks of satellites. We conclude that the detection of coherent rotation in the satellite population in current observational samples is not robust. We compare our data to the Λ CDM Millennium simulations populated with galaxies according to the semi-analytic model of Guo et al. We find excellent agreement with the spatial distribution of satellites in the SDSS data and the lack of a strong signal from coherent rotation.

Key words: galaxies: haloes - galaxies: abundances - galaxies: statistics - dark matter

1 INTRODUCTION

It has been known for decades that the 11 “classical” satellites of the Milky Way (MW) define a thin plane (Lynden-Bell 1976) and that some of the fainter satellites, tidal streams and young globular clusters have an anisotropic distribution reminiscent of this plane (Metz, Kroupa & Jerjen 2009; Pawlowski, Pflamm-Altenburg & Kroupa 2012). Most of the members of this “disk of satellites” have a common rotation direction and it has been claimed that the plane is a rotationally stabilized structure (Metz, Kroupa & Libeskind 2008; Pawlowski & Kroupa 2013). Similarly, the spatial distribution of satellites around Andromeda is also thought to be anisotropic (Koch & Grebel 2006; McConnachie & Irwin 2006), with 15 out of 27 satellites observed by the Pan-Andromeda Archaeological Survey (PAndAS; McConnachie et al. 2009) located in a very thin plane (Ibata et al. 2013), with 13 out of these 15 satellites having negative observed radial velocities (i.e. pointing towards us; Ibata et al. 2013).

Anisotropies in the distribution of satellites are a clear prediction of the Λ cold dark matter (Λ CDM) paradigm (Libeskind et al. 2005; Zentner et al. 2005; Libeskind et al. 2009, 2011; Deason et al. 2011; Wang, Frenk & Cooper

2013). Such flattened satellite distributions, dubbed “great pancakes”, can arise from the infall of satellites along the spine of filaments (Libeskind et al. 2005), which in turn determine the preferential points at which satellites enter the virial radius of the host halo (Libeskind et al. 2011, 2014). Correlated accretion along filaments has also been ascribed by Deason et al. (2011) as the cause of the satellite anisotropies observed in the ‘GIMIC’ gasdynamic simulation (Crain et al. 2009); they found a polar alignment of satellite disks (with more than 10 bright members) for 20% of the cases. The flattening effects of anisotropic accretion are greatly enhanced in the case when subhaloes are accreted in groups (Li & Helmi 2008), though such occurrences are rare for bright satellites and only become more frequent for less massive subhaloes (Wang, Frenk & Cooper 2013). The imprint of anisotropic accretion is retained in the dynamics of satellites, with a significant population of subhaloes co-rotating with the spin of the host halo (Libeskind et al. 2009; Lovell et al. 2011, for galactic haloes; Shaw et al. 2006; Warnick & Knebe 2006 for cluster mass haloes).

Although flattened satellite distributions are common in Λ CDM, the degree of flattening of the MW and Andromeda satellites is atypical. Wang, Frenk & Cooper (2013) found that 5 – 10% of satellite systems are as flat as the MW’s 11 classical satellites but, when the requirement that the veloc-

* E-mail : m.c.cautun@durham.ac.uk

ities of at least 8 of the 11 satellites should point within the narrow angle claimed by Pawlowski & Kroupa (2013) for the Milky Way satellites, this fraction decreases to $\sim 1\%$. In the case of Andromeda’s thin satellite plane, Bahl & Baumgardt (2014) found that, while similar spatial distributions of satellites are quite common in Λ CDM, there is only a 2% chance that 13 out of the 15 members in the plane share the same sense of rotation. In a similar study, Ibata et al. (2014b) found an even lower occurrence rate for Andromeda’s thin plane in Λ CDM simulations.

The presence of such highly flattened satellite systems in the Local Group (LG) raises an important question: are such systems ubiquitous around other galaxies, or are they a consequence of the large-scale environment in which the LG is located? The crucial role of environment in determining the properties of the LG was illustrated by Forero-Romero et al. (2011) who, using constrained simulations of the local cosmological volume, found that LG-analogues have highly atypical formation times, assembly histories and times since last major merger when compared to a sample of similar mass halo pairs.

Studies of large samples of galaxies are limited to investigating anisotropies in the satellite distribution with respect to preferential axes defined by the projected galaxy light. For example, late-type galaxies have satellite distributions that are close to isotropic, while the satellites of early-type galaxies are aligned with the major axis of the galaxy’s light (Brainerd 2005; Yang et al. 2006; Bailin et al. 2008; Agustsson & Brainerd 2010; Guo et al. 2012; Nierenberg et al. 2012). Such studies have limited power to constrain the full flattening of the satellite distribution when such anisotropies are uncorrelated, or only weakly correlated, with the light distribution of the central host.

Recently, Ibata et al. (2014a, hereafter Ibata14) analysed correlations in the velocities of satellite galaxies observed on opposite sides of their central host. For a sample selected from SDSS (Abazajian et al. 2009), they found the most significant effect for an opening angle of $< 8^\circ$, for which 20 out of 22 satellite pairs have anticorrelated velocities, suggestive of a rotating disk that contains $\sim 50\%$ of the satellite population. Ibata et al. (2014a) reported a significance of 4σ for a null hypothesis of an isotropic satellite distribution. They found no such effect in the Millennium II Λ CDM simulations.

In this study we compare the angular distribution of satellites around external galaxies with the predictions of the Guo et al. (2011) semi-analytic model of galaxy formation model implemented in the Millennium (MS; Springel et al. 2005) and Millennium II (MS-II; Boylan-Kolchin et al. 2009) simulations. We make use of both spectroscopic and photometric SDSS data, limiting our analysis to systems of isolated galaxies with at least one spectroscopic satellite. We use the axis connecting the position of the brightest spectroscopic satellite to its host galaxy to measure the angles at which other satellites appear on the sky. The distribution of this angle is sensitive to anisotropies in the spatial distribution of satellites, as we show using a simple disc model. We compare the resulting angular distribution of satellites with Λ CDM predictions for different central host luminosities and find very good agreement between the two. We also show that the excess of satellite pairs with anticorrelated velocities found by Ibata14 is not robust to changes in sample

selection and conclude that the known kinematics of satellites are not in disagreement with Λ CDM predictions.

The paper is organised as follows: Sec. 2 introduces the observational and simulation data, as well as the selection criteria used to identify isolated galaxies and their satellites; in Sec. 3 we obtain the angular distribution of SDSS satellites and compare the results with Λ CDM predictions; Sec. 4 is devoted to studying kinematical signatures of satellite disks and on revisiting the excess of satellite pairs with anticorrelated velocities; we conclude with a short discussion and summary in Sec. 5.

2 DATA AND SAMPLE SELECTION

We identify isolated galaxies and count their satellites using the methods described by Wang & White (2012, hereafter WW12; see also Wang et al. 2014). We now briefly introduce these methods and describe the datasets that we used.

2.1 SDSS isolated galaxy sample

We select isolated primary galaxies from the New York University Value Added Galaxy Catalogue (NYU-VAGC) 1 (Blanton et al. 2005), which is based on the Seventh Data Release of the SDSS (SDSS/DR7; Abazajian et al. 2009). We require that these galaxies should be brighter than any companion lying within projected radius of $r_p = 0.5$ Mpc and having line-of-sight velocity difference $c|\Delta z| < 1500$ km/s. In order to match the selection criteria used by Ibata14, the results presented in Sec. 4 use only this sample of isolated primaries.

For the analysis in Sec. 3 we apply a further isolation selection criterion that takes into account the fact that the SDSS spectroscopic sample is incomplete due to fibre-fibre collisions. To prevent primaries being falsely identified as isolated because of incompleteness in the spectroscopic catalogue, we search for further companions using the photometric SDSS catalogue. We reject primary candidates if they have a photometric companion which is not in the spectroscopic catalogue but satisfies the position and magnitude cuts given above and the probability that its redshift is equal to or less than the primary is larger than 10%. For this last step we use the photometric redshift distributions from Cunha et al. (2009).

2.2 SDSS satellite galaxy sample

For the analysis described in Sec. 3 we first split the isolated galaxy sample into three subsamples according to their absolute r-band magnitudes. We use three bins centred on $M_r = -23, -22$ and -21 , each of width $\Delta M_r = 1$, as shown in Table 1. We count as satellites all galaxies within a projected radius in the range 20 kpc to the virial radius, R_v , with $R_v = 500, 315$ and 150 kpc, which correspond to the median virial radii of haloes hosting the galaxies found in each of our luminosity bins¹. Out of all

¹ We used the Guo et al. (2011) MS catalogue to find the median virial radii of galaxies in each magnitude range. The virial radius of the brightest bin is larger than 500 kpc but we adopted this

Table 1. The number of isolated galaxies with at least one associated spectroscopic satellite. The MS and MS-II data correspond to the average number of isolated galaxies per line-of-sight, because multiple lines-of-sight were used to construct the mock data.

host M_r range	SDSS	MS	MS-II
$-22.5 \geq M_r \geq -23.5$	4 211	16 430	111
$-21.5 \geq M_r \geq -22.5$	16 532	112 100	938
$-20.5 \geq M_r \geq -21.5$	8 519	235 360	2 010

the isolated primaries, we keep only those which have at least one spectroscopic satellite within projected distance between 20 kpc and R_v and having a line-of-sight velocity difference, $c|\Delta z| < 300$ km/s. The number of isolated galaxies satisfying these criteria is given in Table 1.

We are only interested in isolated primaries with spectroscopically associated satellites since we want to determine a preferential axis that can be used to probe anisotropies in the satellite distribution. The relative position of the satellite with respect to its host represents such a reference axis, \mathbf{x}_{BS} , since the satellite is more likely to be found along the direction where there is an excess of satellites. If an isolated galaxy has two or more spectroscopic satellites associated with it, we choose the brightest one because the brightest satellites show the largest degree of anisotropy (Wang, Frenk & Cooper 2013; Libeskind et al. 2014).

To compute the angular distribution of satellites we use the SDSS/DR8 photometric catalogue (Aihara et al. 2011), which we correct statistically for background contamination (see WW12 for details). For each isolated galaxy, we identify objects brighter than apparent magnitude $r = 21$ that are within a projected distance between 20 kpc and R_v . For each of these potential satellites we calculate the angle, θ_{BS-S} , with respect to the reference axis, \mathbf{x}_{BS} , of the system. We then count the number of satellites as a function of the angle θ_{BS-S} . This count excludes the brightest satellite, for which $\theta_{BS-S} = 0^\circ$ by definition. For each bin in θ_{BS-S} , we subtract the average number of galaxies brighter than $r = 21$ expected in this area of the sky, as estimated from the survey as a whole. The excess counts with respect to a homogeneous galaxy background are assumed to be satellites physically associated with the primary galaxy. Finally, results for different primaries can be averaged after making completeness, volume and edge corrections, as described in WW12.

The selection of satellites in the sample used in Sec. 4 is restricted to galaxies with spectroscopic redshifts following the criteria described in Ibata14. For each isolated primary we identify galaxies that are at least $\Delta M_r^{\text{Sat-Cen}} = 1$ mag. fainter than the primary and lie within a projected distance between 20 kpc and $R_{\text{max}} = 150$ kpc. We further require that the line-of-sight velocity difference of the satellite be $35 \text{ km/s} \leq c|\Delta z| \leq V_0 \exp(-(R/300 \text{ kpc})^{0.8})$, where $V_0 = 300$ km/s and R is the projected distance from the primary of the satellite candidate. We also limit the analysis to primary galaxies in the redshift range 0.002 to $z_{\text{max}} = 0.05$. The final sample consists of all primaries with two or more satellites satisfying the above selection criteria. To assess

value since it corresponds to the projected radius used to identify isolated primaries.

the robustness of the results we vary each of the selection criteria in turn.

2.3 Mock Λ CDM galaxy catalogue

To construct mock catalogues, we use the semi-analytic galaxy formation model of Guo et al. (2011) implemented in the MS (Springel et al. 2005) and MS-II (Boylan-Kolchin et al. 2009). The semi-analytic model has been calibrated to reproduce the stellar mass, luminosity and autocorrelation functions of low redshift galaxies as inferred from SDSS. The abundance and radial distribution of satellites predicted by the model is in very good agreement with SDSS data (WW12; Wang et al. 2014). The two simulations, the high resolution MS-II and the lower resolution but larger volume MS, complement each other well for the purposes of this study. The Guo et al. (2011) data are publicly available at <http://www.mpa-garching.mpg.de/millennium>.

We create the simulated catalogues by projecting galaxies along random sightlines and assigning a redshift according to their line-of-sight distance and peculiar velocity. We add a Gaussian random velocity error of $\sigma = 15$ km/s to the radial velocity to simulate the typical SDSS spectroscopic redshift error. We then apply the same host isolation and satellite identification criteria as in our SDSS data to obtain a mock sample of isolated primaries and their satellites. In Sec. 4 we use only satellites brighter than an absolute magnitude of $M_r = -17$. In Sec. 3 we find the angular distribution of satellites by counting all the satellites brighter than $r = 21$ lying within projected distance between 20 kpc and R_v , from which we subtract the average galaxy background of the mock catalogue. When stacking the counts in each primary magnitude bin, we assign weights to the primaries so as to obtain the same redshift distributions in our mock and SDSS samples. We obtain the same average number of satellites per primary for both mock and real data. We create multiple mock catalogues using 1000 and 25 random sightlines from the MS-II and MS respectively.

3 SPATIAL DISTRIBUTION OF SATELLITES

In this section we characterise the anisotropies of the satellite distribution around a large number of primary galaxies. For each system, we define a reference axis, \mathbf{x}_{BS} , given by the relative position of the brightest satellite with respect to the primary galaxy, as described in Sec. 2.2. This reference axis points towards the direction where an excess of satellites is expected on average, if such an excess exists. We first test this approach using a simplified disk model, following which we apply the method to both observations and mock catalogues.

3.1 A simplified disk model

To illustrate our approach we use the MS data to construct a simple model where a fraction, f_{disk} , of the satellites is distributed on a disk of 30 kpc thickness while the remaining satellites are distributed isotropically. We first identify the ‘friends-of-friends’ (FOF) group to which each primary galaxy belongs. Members of the FOF group other than the primary are then randomly assigned to be part of the disk

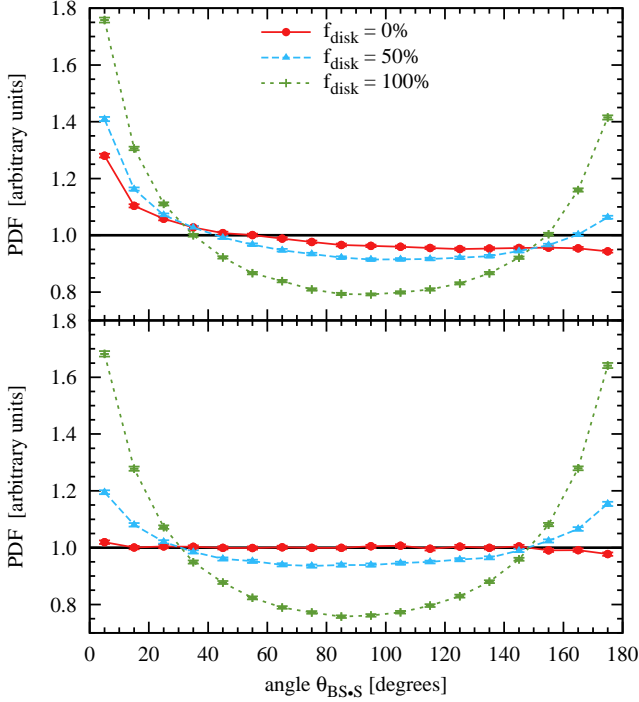


Figure 1. *Top panel:* the probability distribution function (PDF) of the angle, $\theta_{BS,S}$, of satellites with respect to the line joining the primary to the brightest satellite in our simplified disk models. In these models a fraction of satellites, f_{disk} , of 0%, 50% and 100% are randomly assigned to disks, and the remaining are isotropically distributed around the primary galaxy. *Bottom panel:* as above, but only for the case where the brightest satellite is part of the same FOF group as the central galaxy.

or of the isotropic population, depending on the value of f_{disk} . Finally, the satellites are spatially rearranged into the disk and isotropic populations such that they have the same radial distribution with respect to the primary as in the undisturbed case.

We create new mock catalogues using these disk models, which we analyse in the same way as the SDSS data. The resulting angular distribution function of satellites is shown in the top panel of Fig. 1, where the y-scale is chosen such that a uniform distribution would correspond to a value of 1. Comparing models with different disk fractions, it is clear that the distribution of angles is sensitive to anisotropy in the satellite spatial distribution. The first striking result is the asymmetry between the $\theta_{BS,S} = 0^\circ$ and $\theta_{BS,S} = 180^\circ$ points, which is unexpected given that, by construction, the satellite distributions have cylindrical symmetry. The asymmetry is due to clustering around interloper galaxies, which although not part of the same FOF group as the primary, are close enough in redshift ($c|\Delta z| < 300$ km/s) to be identified as satellites according to our selection criteria. To quantify this effect we repeat the analysis requiring that the brightest satellite of each primary (which defines the reference axis) be part of the same FOF group. The result is displayed in the bottom panel of Fig. 1, which shows that the curves in this case are symmetric around $\theta_{BS,S} = 90^\circ$.

In addition to clustering around interloper galaxies, there is also clustering around the brightest satellite within an FOF group. This latter effect is not captured in our sim-

plified model where the azimuthal angles are randomized, hence the symmetric curve in the bottom panel of Fig. 1. In the real case we expect this additional clustering around the brightest satellites to enhance further the asymmetry of the angular distribution of satellites over and above that seen in the top panel of Fig. 1.

The effect of clustering around the brightest satellite is particularly evident for $\theta_{BS,S} < 90^\circ$, which suggests that we should use the $\theta_{BS,S} > 90^\circ$ part of the curve for quantifying anisotropy. For example, the disk model with $f_{disk} = 0\%$ shows a nearly flat curve for $\theta_{BS,S} > 90^\circ$, as expected for an isotropic distribution. In contrast, the model with $f_{disk} = 50\%$ shows 16% more satellites at $\theta_{BS,S} = 180^\circ$ than at $\theta_{BS,S} = 90^\circ$. The difference between the values for the two angles increases to 86% for $f_{disk} = 100\%$. This suggests that, with good statistics, i.e. a large enough sample of primaries with at least one spectroscopic satellite, the method can easily quantify the average spatial anisotropy of the satellite distribution. Compared to previous studies (discussed in Sec. 1), our analysis has the advantage that it is independent of the correlation between the light distribution of the primary galaxy and the anisotropy of the satellite distribution.

3.2 The angular distribution of satellites in the SDSS and mock catalogues

The angular distribution of satellites in the SDSS is given in Fig. 2, with each panel showing the results for a different range of primary magnitudes. We use bootstrap resampling to estimate errors for both observational and mock data. For the latter, this accounts for the fact that the same object can be seen multiple times along different sightlines. With the exception of the faintest primary sample, where the errors are comparable to the signal, the data clearly exhibits the telltale sign of an anisotropic distribution: more objects at $\theta_{BS,S} = 180^\circ$ than at $\theta_{BS,S} = 90^\circ$.

Considering first the results from the mock catalogues, it is reassuring that the MS and MS-II, which differ in mass resolution by a factor of 125, give consistent data. This suggests that our results are unaffected by resolution effects or by the treatment of orphan galaxies (i.e. satellites whose dark matter halos have been stripped). The only notable, although small, difference between the two simulations is in the faintest magnitude bin where most of the signal is due to satellites with $M_r \gtrsim -16$ which are not properly resolved in the MS. We have also tested the effect of excluding orphan galaxies from the analysis and find that, in the case of the MS-II, the results hardly change.

The main conclusion from Fig. 2 is that the SDSS data agree well with the results from the mocks based on a semi-analytic model of galaxy formation in Λ CDM. This shows that, contrary to recent claims (e.g. Kroupa 2012), there is no conflict between the observed spatial anisotropies in the satellite distribution and the Λ CDM model. In fact, as emphasized amongst others by Libeskind et al. (2005) and Wang, Frenk & Cooper (2013), such anisotropies are actually *expected* in Λ CDM.

The simulations predict 20% more satellites at $\theta_{BS,S} = 180^\circ$ than at $\theta_{BS,S} = 90^\circ$ for the two brightest bins, and 17% more for the faintest primary sample. If we were to interpret these results in the light of the simplified disk model

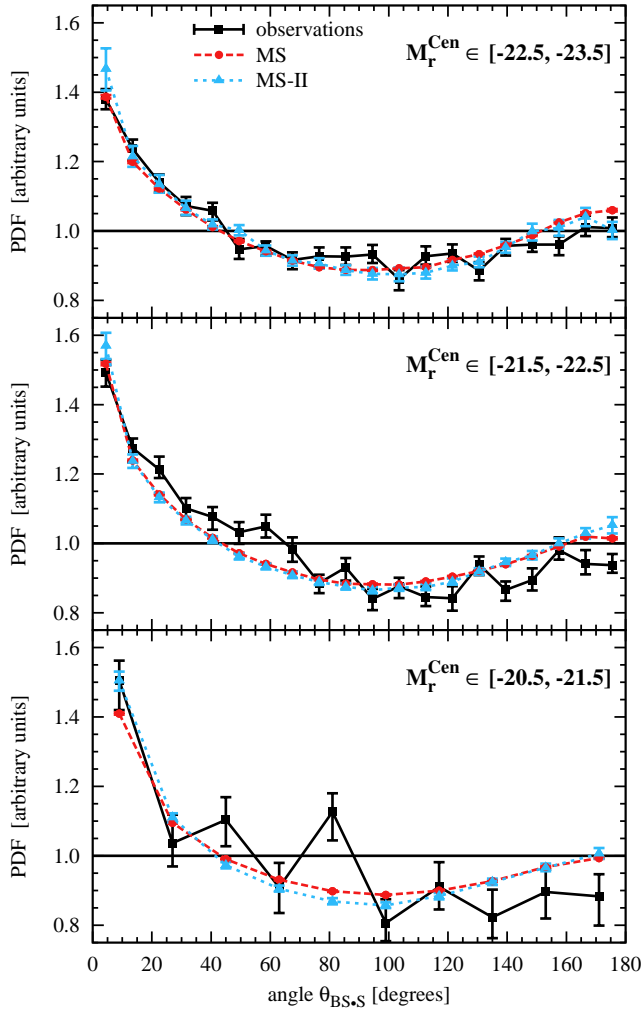


Figure 2. The probability distribution function (PDF) of the angle, $\theta_{BS,S}$, of satellites with respect to the line joining the primary to the brightest satellite. Results are shown for primaries in three magnitude ranges: $-22.5 \geq M_r^{\text{Cen}} \geq -23.5$ (top), $-21.5 \geq M_r^{\text{Cen}} \geq -22.5$ (centre) and $-20.5 \geq M_r^{\text{Cen}} \geq -21.5$ (bottom). The solid black curve is for the observational data, while the red and blue curves are for the MS and MS-II respectively.

introduced in Fig. 1, this would suggest that, on average, around $\sim 50\%$ of the satellites are in a relatively thin plane. Cosmological simulations show that these planar structures arise from the anisotropic infall of satellite galaxies along filaments, which leads to the formation of flattened, pancake-like satellite distributions (Libeskind et al. 2005).

4 THE ROTATION OF PLANAR STRUCTURES

The motion of satellites around their primary galaxy, as predicted by Λ CDM, is not random, but retains a signature of their anisotropic infall (Lovell et al. 2011). This is illustrated in Fig. 3, where we show the PDF of $\cos \theta_{H,S}$, the cosine of the angle between the halo spin and the orbital momentum of the satellites. These results were obtained by analysing the MS-II real space data for central galaxies in the mag-

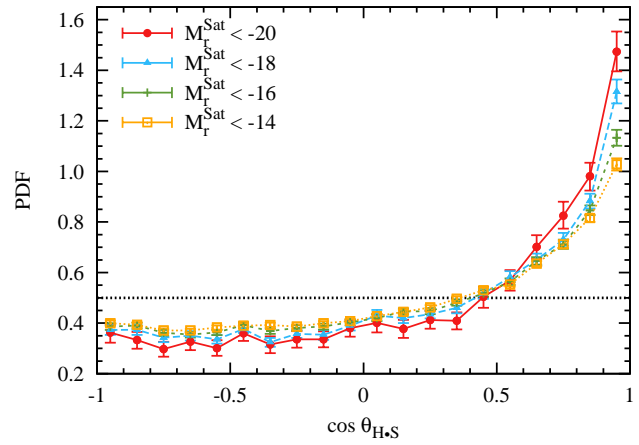


Figure 3. The probability distribution in the MS-II simulation of $\cos \theta_{H,S}$, the cosine of the angle between the host halo spin and the orbital momentum of its satellites. The black horizontal line corresponds to a uniform distribution.

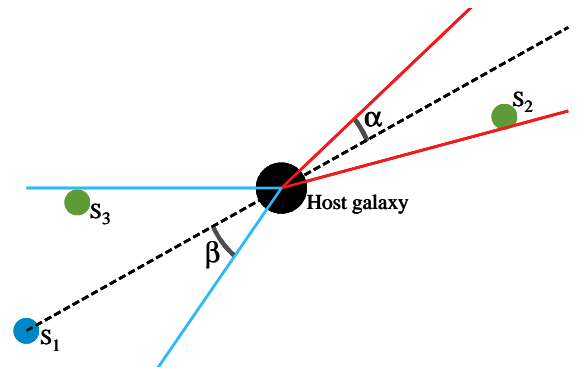


Figure 4. Definition of the tolerance angles, α and β , used to characterise satellite pairs on opposite sides (S_1S_2) and on the same side (S_1S_3) of primary galaxy, respectively.

nitude range $-20 \geq M_r^{\text{Cen}} \geq -23$. They demonstrate that satellite galaxies rotate preferentially in the same direction as their host halo, corroborating the results of Lovell et al. (2011), who analysed the six Milky Way mass halos of the Aquarius project (Springel et al. 2008). The correlation is strongest for the brightest satellite galaxies. For this sample, the same sense of rotation is shared, on average, by 3 times more satellites than expected from a random distribution. The figures indicate that $\sim 15\%$ of the satellites share the same direction of rotation to within 25° , i.e. $\cos \theta_{H,S} \geq 0.9$. While this represents a significant fraction of the population, it falls short of the $\sim 50\%$ fraction found in the SDSS by Ibata14.

To investigate the reported discrepancy between observations and Λ CDM predictions, we have reanalysed the SDSS data used by Ibata14 and extended this kind of analysis in order to obtain better statistics. We are interested in the number of satellite pairs with correlated and anticorrelated line-of-sight velocities as a function of a tolerance angle that characterises the angular separation of the pair, as illustrated in Fig. 4. The tolerance angle, α , refers to satellite pairs on diametrically opposite sides of the primary, fol-

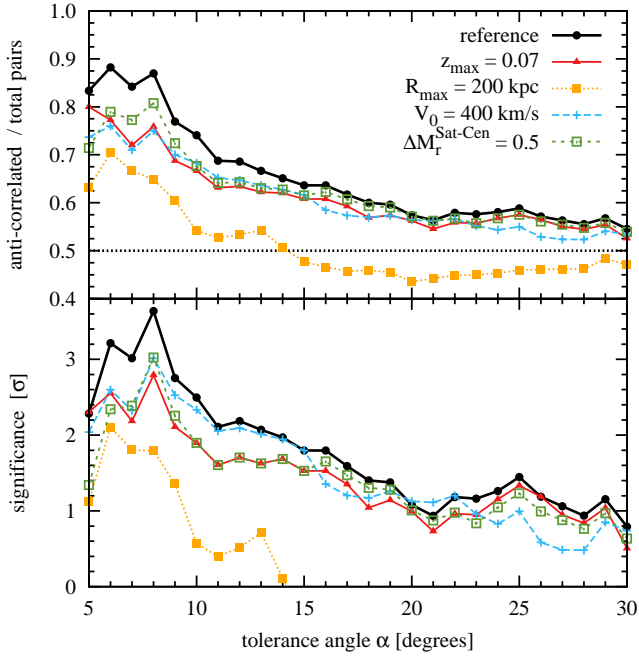


Figure 5. *Top panel:* the excess of satellite pairs with anticorrelated velocities as a function of the tolerance angle, α , for diametrically opposite pairs. The colour curves show differences from the reference result (solid black) when varying the sample selection criteria, one at a time. Following Ibata14, the reference result assumes $z_{\max} = 0.05$, $R_{\max} = 150$ kpc, $V_0 = 300$ km/s and $\Delta M_r^{\text{Sat-Cen}} = 1$. *Bottom panel:* the significance of the excess of satellite pairs with anticorrelated velocities compared to the null hypothesis of equal numbers of pairs with correlated and anticorrelated velocities.

lowing the same convention as Ibata14, while the tolerance angle, β , refers to pairs on the same side of the host.

4.1 Diametrically opposed satellite pairs

To begin with our analysis follows the exact sample selection criteria described by Ibata14 (see Sec. 2 for details). At a tolerance angle, $\alpha = 8^\circ$, we were able to recover only 20 pairs of diametrically opposite satellites compared to the 22 pairs reported by Ibata14. This discrepancy is likely due to the use of different versions of the NYU-VAGC catalogue². Our original sample missed two pairs with anticorrelated velocities that appear in the sample of Ibata14, corresponding to rows 1 and 18 in their Table 1. Using Vizier, we found the satellite pair in row 18 in another catalogue, but we could not identify one of the satellites of the pair in row 1. Nevertheless, we have chosen to include both these pairs in our sample. We also found an additional pair with $\alpha < 8^\circ$, which has correlated velocities, that does not appear in the Ibata14 sample.

² There is an ambiguity regarding the catalogue used by Ibata14 since the NYU-VAGC website they referenced contains a multitude of catalogues. After trying several of them, we settled on the one which gives absolute magnitudes closest to the values given in Table 1 of Ibata14. Nevertheless, there is a ~ 0.03 scatter between the absolute magnitudes in our catalogue and those quoted by Ibata14.

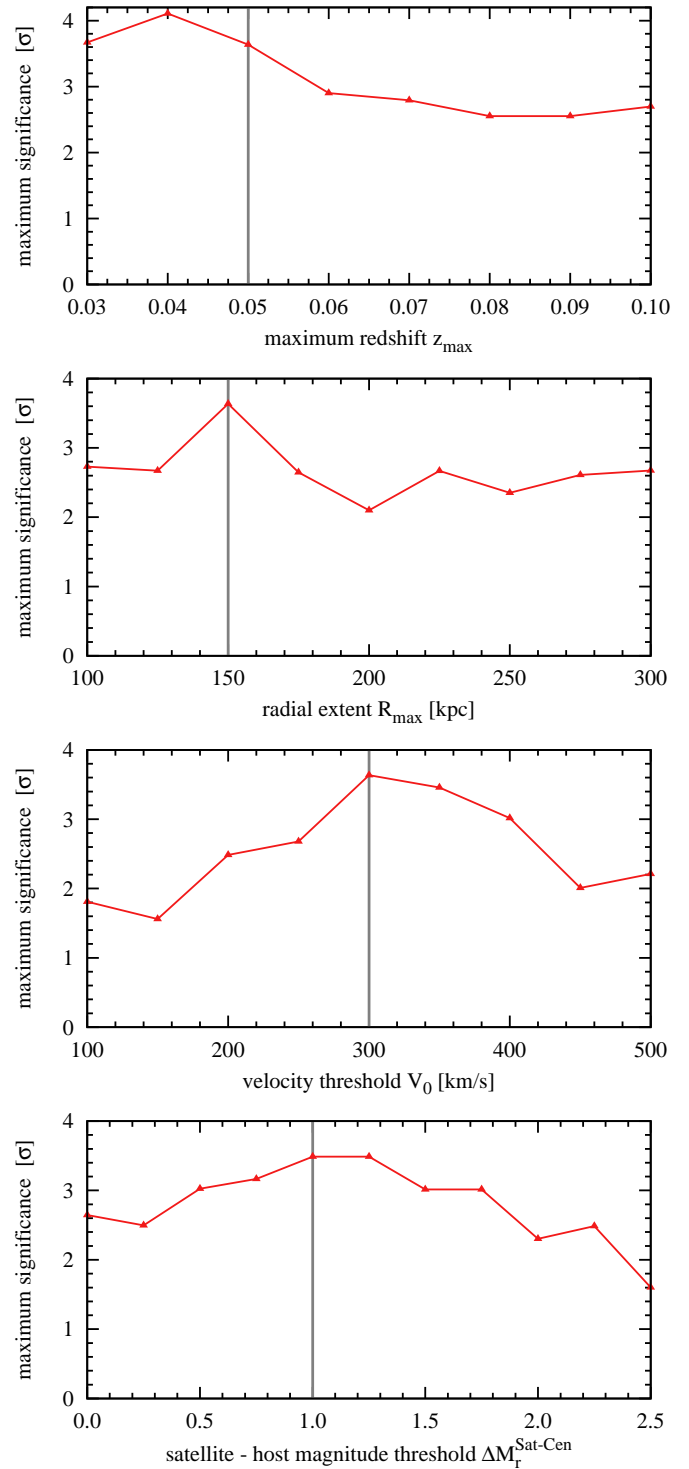


Figure 6. The maximum significance of the excess of satellite pairs with anticorrelated velocities over the tolerance angle range $5^\circ \leq \alpha \leq 30^\circ$, as a function of different sample selection criteria. For all cases we retain the same selection parameters as in the reference case of Ibata14 but vary, in turn, the maximum redshift (top panel), the radial extent of the volume over which satellites are found (second panel), the maximum velocity difference with respect to the primary (third panel), and the magnitude difference between primary and satellite (bottom panel). The grey lines indicate the choices made in the reference model of Ibata14.

The excess of pairs with anticorrelated velocities and its significance as a function of the tolerance angle, α , is shown by the thick black line in Fig. 5. The significance of the excess is evaluated as the sigma-value corresponding to the probability of obtaining such an excess for a binomial distribution of mean 0.5. The inclusion of an additional pair with correlated velocities in our sample results in a smaller excess of anticorrelated pairs than found by Ibata14 and a correspondingly lower statistical significance. The most significant excess is found at $\alpha = 8^\circ$ and corresponds to a 3.6σ significance, compared to a maximum significance of 4σ reported by Ibata14 at the same tolerance angle.

Fig. 5 also shows how the excess of anticorrelated velocity pairs changes when the sample selection criteria are relaxed. We vary one parameter of the selection criteria at a time, keeping the remaining parameters at their reference values as given in Sec. 2. In all cases we find that the excess of anticorrelated pairs decreases as does the corresponding maximum significance of the excess.

We explore further the sensitivity of the excess of anticorrelated velocity pairs by systematically varying, one at a time, some of the parameters used to select the sample. In each case, we determine the maximum significance of the signal over the range of tolerance angles, $5^\circ \leq \alpha \leq 30^\circ$. With few exceptions, the maximum significance is found for $\alpha = 8^\circ$. The maximum significance as function of some of the main parameters in the selection criteria is plotted in Fig. 6. For clarity, the reference values for each parameter are shown as a vertical grey line. We find that small variations in the sample selection parameters can lead to a significant reduction in the significance of the observed excess of anticorrelated velocity pairs. Except for a few values, the maximum significance is below the 3σ level.

The choices made by Ibata14 reflect various compromises (R. Ibata, private communication). The maximum redshift cut, $z_{\max} = 0.05$, was chosen because this value has been commonly used in similar studies to avoid including very bright satellites. The search radius, $R_{\max} = 150$ kpc, was chosen to match the M31 PAnDAS survey, while the velocity threshold, $V_{\max} = 300$ km/s, corresponds to twice the central velocity dispersion of Andromeda. The maximum magnitude difference, $\Delta M_r^{\text{Sat-Cen}} = 1$, between satellites and the central galaxy was chosen in order to discard objects that are too close in brightness to the host.

These choices, of course, are to some extent arbitrary. For example, increasing the maximum redshift range from $z_{\max} = 0.05$ to 0.07 adds mainly bright primaries with absolute r-band magnitudes in the range $[-22.6, -22.0]$ which already includes more than half of the primaries in the reference sample. Similarly, increasing the maximum radius used to identify satellites from $R_{\max} = 150$ kpc to 200 kpc is not unreasonable given that most of the galaxies in our sample occupy halos with a virial radius larger than 200 kpc. The sensitivity of the results to the details of the sample selection lead us to conclude that the detection of systemic rotation in the satellite population with current observational samples is not robust.

4.2 Same-side satellite pairs

If the excess of pairs with *anticorrelated* velocities on opposite sites of the host were attributable to rotating disks of

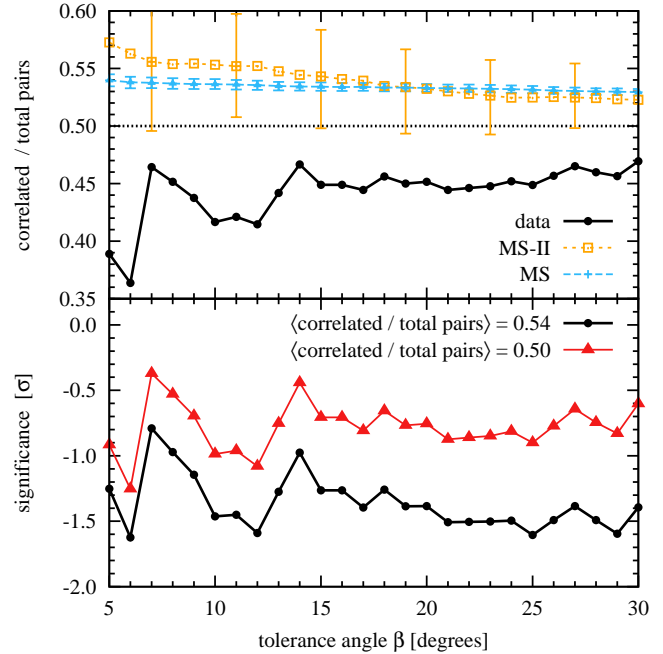


Figure 7. *Top panel:* the excess of satellite pairs with correlated velocities as a function of the tolerance angle, β , for pairs found on the same side of the primary. We compare the observational data (solid black) with results from the MS (blue crosses) and MS-II (orange open squares). The signature of rotating disks of satellites is an excess of pairs with correlated velocities. In contrast, the data show a small deficit of pairs with correlated velocities. The error bars for the MS and MS-II data show 1σ bootstrap uncertainties. *Bottom panel:* the significance of the excess of satellite pairs with correlated velocities compared to the MS predictions (circles; mean expectation of 0.54) and to a uniform distribution (triangles; mean expectation of 0.5). The negative values for the significance reflect the fact that instead of an excess, we find a deficit of correlated pairs.

satellites, an equal but opposite excess of *correlated* velocities would be expected for pairs of satellites on the same side of the primary. This provides an independent test of the significance of the result reported in the previous section. For same-side satellite pairs we use the same selection criteria as described in Sec. 2 and in Ibata14, but also require the projected distance between satellites to be greater than 20 kpc to ensure that our sample is not affected by very tightly bound binary systems.

Fig. 7 shows the fractional abundance of correlated velocities and its significance as a function of the tolerance angle, β , for same-side satellite pairs. Instead of the expected excess, we find a small deficit of pairs with correlated velocities, although the result is consistent, within 1σ , with a uniform distribution and only marginally inconsistent, $\sim 1.5\sigma$, with the results from the mock catalogue. Even in the absence of disks, the MS and MS-II simulations predict a slight excess, 54%, of correlated velocity pairs, which may be due to binary satellites orbiting around the brighter primary. Note that for diametrically opposite satellite pairs the simulations predict an equal number of anticorrelated and correlated velocity pairs. The idea of rotating disks of satellites is disfavoured by the lack of excess of same-side pairs with correlated velocities and supports the low signifi-

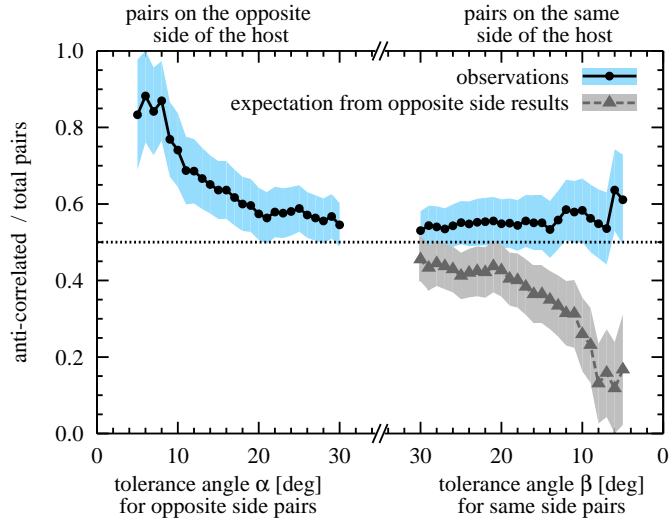


Figure 8. Comparison of the excess of satellite pairs with anticorrelated velocities for pairs diametrically opposite (left-half) and on the same side (right-half) of the primary. The observational results are shown by the filled circles. The filled triangles show the expected signal if the results found for diametrically opposite pairs were indicative of a rotating disk of satellites (it is a mirror image of the left-half results with respect to the $y = x$ diagonal). The shaded region shows the 1σ uncertainty.

cance of the excess of anticorrelated velocities for opposite-side pairs found in the preceding section.

5 CONCLUSION AND DISCUSSION

In the first part of this study we characterised the spatial distribution of satellites in a large sample of SDSS galaxies. Our analysis focused on isolated primaries that have one or more satellites with spectroscopic redshifts. We used the photometric catalogue of SDSS/DR8 galaxies to count the number of satellites as a function of the angle they subtend relative to a reference axis defined by the brightest satellite. We considered three samples of primary galaxies centred on absolute magnitudes of $M_r = -23, -22$ and -21 . We found a clear signal of anisotropy in the spatial distributions of satellites of the two brightest samples of primaries, while for the faintest sample the uncertainties are of the same order as the expected signal. We compared the observational data to the predictions of the semi-analytic galaxy formation model of Guo et al. (2011) implemented in the Λ CDM Millennium and Millennium-II cosmological simulations, and find very good agreement between the observations and the theoretical predictions.

In the second part of this study we extended the analysis of Ibata14 to explore if the anisotropy we detected could be related to the rotating disks of satellites claimed by these authors. We concluded that the observational sample is not robust enough to detect such disks. This result is also consistent with Λ CDM where rotating satellite disks do exist (Lovell et al. 2011) but not to the extent reported by Ibata14. In particular, we found the excess of diametrically opposite satellite pairs with anticorrelated velocities seen by Ibata14 to be very sensitive to the sample selection criteria. Small variations from the reference criteria employed by

these authors lead to smaller excesses of anticorrelated pairs and, almost invariably, to a reduced significance, which in many cases is well below 3σ . We can think of no good physical reason why relaxing some of the sample selection criteria would lead to a lower signal and conclude that the detection of rotating satellite disks in the SDSS data is not robust.

To test further if the reported excess of anticorrelated velocities among satellites on opposite sides of the primary could originate from a large fraction of systems having rotating disks of satellites, we compared it to the expected excess of correlated velocities among satellites on the same side of their respective primaries. Using similar selection criteria to those used by Ibata14 to define the opposite-side pairs, we found no excess of correlated velocities in same-side pairs in the SDSS sample.

The results for opposite and same-side satellite systems are summarised in Fig. 8, which shows the fraction of anticorrelated pairs of satellites on either the opposite or the same side of their host primary. Filled circles show the actual measurements on both sides, while on the right half, grey triangles denote the expected signal for same-side pairs if the excess of anticorrelated velocities measured for opposite-side pairs were indicative of rotating disks. The measurements for same-side pairs are clearly in disagreement with this hypothesis, especially at small tolerance angle, β , where the signal of a rotating disk is expected to be maximal. This lack of any rotation signal among same-side satellites and the discrepancy with the reported signal from opposite-side satellites further weakens the evidence for universally rotating satellite systems.

The spatial and kinematic distributions of the satellites around the Milky Way and, more recently, around Andromeda have been claimed to pose a serious challenge to the Λ CDM model (e.g. Kroupa, Theis & Boily 2005; Pawlowski, Pflamm-Altenburg & Kroupa 2012; Ibata et al. 2013) on the grounds that Λ CDM haloes seldom have satellite distributions that are as flattened and showing the same degree of coherent rotation as found in the Local Group (Wang, Frenk & Cooper 2013; Bahl & Baumgardt 2014; Ibata et al. 2014b). From our analysis of the spatial and kinematic distributions of the satellites around a large sample of SDSS galaxies, we find instead a very good agreement with Λ CDM predictions. This suggests that the satellite populations of the MW and Andromeda are outliers, rather than symptomatic of a failure of the Λ CDM paradigm.

ACKNOWLEDGEMENTS

We are grateful to Rodrigo Ibata for useful and helpful discussions; and to Shaun Cole, Wojciech Hellwing and Qi Guo for discussions during the preliminary stages of the project. This work was supported in part by ERC Advanced Investigator grant COSMIWAY [grant number GA 267291] and the Science and Technology Facilities Council [grant number ST/F001166/1, ST/I00162X/1]. WW is supported by JRF grant number RF040353. This work used the DiRAC Data Centric system at Durham University, operated by ICC on behalf of the STFC DiRAC HPC Facility (www.dirac.ac.uk). This equipment was funded by BIS National E-infrastructure capital grant ST/K00042X/1, STFC capital grant ST/H008519/1, and STFC DiRAC Operations

grant ST/K003267/1 and Durham University. DiRAC is part of the National E-Infrastructure. This research was carried out with the support of the “HPC Infrastructure for Grand Challenges of Science and Engineering” Project, co-financed by the European Regional Development Fund under the Innovative Economy Operational Programme.

REFERENCES

- Abazajian K. N. et al., 2009, *ApJS*, 182, 543
 Agustsson I., Brainerd T. G., 2010, *ApJ*, 709, 1321
 Aihara H. et al., 2011, *ApJS*, 193, 29
 Bahl H., Baumgardt H., 2014, *MNRAS*, 438, 2916
 Bailin J., Power C., Norberg P., Zaritsky D., Gibson B. K., 2008, *MNRAS*, 390, 1133
 Blanton M. R. et al., 2005, *AJ*, 129, 2562
 Boylan-Kolchin M., Springel V., White S. D. M., Jenkins A., Lemson G., 2009, *MNRAS*, 398, 1150
 Brainerd T. G., 2005, *ApJ*, 628, L101
 Crain R. A. et al., 2009, *MNRAS*, 399, 1773
 Cunha C. E., Lima M., Oyaizu H., Frieman J., Lin H., 2009, *MNRAS*, 396, 2379
 Deason A. J. et al., 2011, *MNRAS*, 415, 2607
 Forero-Romero J. E., Hoffman Y., Yepes G., Gottlöber S., Piontek R., Klypin A., Steinmetz M., 2011, *MNRAS*, 417, 1434
 Guo Q., Cole S., Eke V., Frenk C., 2012, *MNRAS*, 427, 428
 Guo Q. et al., 2011, *MNRAS*, 413, 101
 Ibata N. G., Ibata R. A., Famaey B., Lewis G. F., 2014a, *Nature*, 511, 563, (Ibata14)
 Ibata R. A., Ibata N. G., Lewis G. F., Martin N. F., Conn A., Elahi P., Arias V., Fernando N., 2014b, *ApJ*, 784, L6
 Ibata R. A. et al., 2013, *Nature*, 493, 62
 Koch A., Grebel E. K., 2006, *AJ*, 131, 1405
 Kroupa P., 2012, *PASA*, 29, 395
 Kroupa P., Theis C., Boily C. M., 2005, *A&A*, 431, 517
 Li Y.-S., Helmi A., 2008, *MNRAS*, 385, 1365
 Libeskind N. I., Frenk C. S., Cole S., Helly J. C., Jenkins A., Navarro J. F., Power C., 2005, *MNRAS*, 363, 146
 Libeskind N. I., Frenk C. S., Cole S., Jenkins A., Helly J. C., 2009, *MNRAS*, 399, 550
 Libeskind N. I., Knebe A., Hoffman Y., Gottlöber S., 2014, *MNRAS*, 443, 1274
 Libeskind N. I., Knebe A., Hoffman Y., Gottlöber S., Yepes G., Steinmetz M., 2011, *MNRAS*, 411, 1525
 Lovell M. R., Eke V. R., Frenk C. S., Jenkins A., 2011, *MNRAS*, 413, 3013
 Lynden-Bell D., 1976, *MNRAS*, 174, 695
 McConnachie A. W., Irwin M. J., 2006, *MNRAS*, 365, 902
 McConnachie A. W. et al., 2009, *Nature*, 461, 66
 Metz M., Kroupa P., Jerjen H., 2009, *MNRAS*, 394, 2223
 Metz M., Kroupa P., Libeskind N. I., 2008, *ApJ*, 680, 287
 Nierenberg A. M., Auger M. W., Treu T., Marshall P. J., Fassnacht C. D., Busha M. T., 2012, *ApJ*, 752, 99
 Pawlowski M. S., Kroupa P., 2013, *MNRAS*, 435, 2116
 Pawlowski M. S., Pflamm-Altenburg J., Kroupa P., 2012, *MNRAS*, 423, 1109
 Shaw L. D., Weller J., Ostriker J. P., Bode P., 2006, *ApJ*, 646, 815
 Springel V. et al., 2008, *MNRAS*, 391, 1685
 Springel V. et al., 2005, *Nature*, 435, 629
 Wang J., Frenk C. S., Cooper A. P., 2013, *MNRAS*, 429, 1502
 Wang W., Sales L. V., Henriques B. M. B., White S. D. M., 2014, *MNRAS*, 442, 1363
 Wang W., White S. D. M., 2012, *MNRAS*, 424, 2574, (WW12)
 Warnick K., Knebe A., 2006, *MNRAS*, 369, 1253
 Yang X., van den Bosch F. C., Mo H. J., Mao S., Kang X., Weinmann S. M., Guo Y., Jing Y. P., 2006, *MNRAS*, 369, 1293
 Zentner A. R., Kravtsov A. V., Gnedin O. Y., Klypin A. A., 2005, *ApJ*, 629, 219